

# ***XMM-Newton* Detection of Hard X-ray Emission in the Nitrogen-type Wolf-Rayet Star WR 110**

Stephen L. Skinner

*CASA, Univ. of Colorado, Boulder, CO 80309-0389*

Svetozar A. Zhekov <sup>1</sup>

*JILA, Univ. of Colorado, Boulder, CO 80309-0440*

Manuel Güdel

*Paul Scherrer Institute, Würenlingen and Villigen, CH-5232 Switzerland*

and

Werner Schmutz

*Physikalisch-Meteorologisches Observatorium Davos, Dorfstrasse 33, CH-7260 Davos Dorf,  
Switzerland*

## **ABSTRACT**

We have used the excellent sensitivity of XMM-Newton to obtain the first high-quality X-ray spectrum of a Wolf-Rayet (WR) star which is not known to be a member of a binary system. Our target, the nitrogen-type star WR 110 (= HD 165688) was also observed and detected with the VLA at four different frequencies. The radio flux density increases with frequency according to a power law  $S_\nu \propto \nu^{+0.64 \pm 0.10}$ , in very good agreement with the behavior expected for free-free wind emission. The radio data give an ionized mass-loss rate  $\dot{M} = 4.9 \times 10^{-5} M_\odot \text{ yr}^{-1}$  for an assumed spherical constant-velocity wind.

The undispersed CCD X-ray spectra reveal strong emission lines from He-like ions of Mg, Si and S. The emission measure distribution shows a dominant contribution from cool plasma with a characteristic temperature  $kT_{cool} \approx 0.5 \text{ keV}$  ( $\approx 6 \text{ MK}$ ). Little or no excess absorption of this cool component above the value expected from the visual extinction is present. We conclude that the bulk of the cool plasma detected by XMM-Newton lies at hundreds of stellar radii or more

---

<sup>1</sup>On leave from Space Research Institute, Sofia, Bulgaria

if the wind is approximately spherical and homogeneous, but it could lie closer to the star if the wind is clumped. If the cool plasma is due to instability-driven wind shocks then typical shock velocities are  $v_s \approx 340 - 550 \text{ km s}^{-1}$  and the average filling factor of X-ray emitting gas in the wind is no larger than  $f \sim 10^{-6}$ .

A surprising result is the unambiguous detection of a hard X-ray component which is clearly seen in the hard-band images and the spectra. This hard component accounts for about half of the observed flux and can be acceptably fitted by a hot optically thin thermal plasma or a power-law model. If the emission is thermal, then a temperature  $kT_{hot} \geq 3 \text{ keV}$  is derived. Such high temperatures are not predicted by current instability-driven wind shock models and a different mechanism is thus required to explain the hard X-rays. We examine several possible mechanisms and show that the hard emission could be accounted for by the WR wind shocking onto a close stellar companion which has so far escaped detection. However, until persuasive evidence for binarity is found we are left with the intriguing possibility that the hard X-ray emission is produced entirely by the Wolf-Rayet star.

*Subject headings:* radio continuum: stars — stars: individual (HD 165688) — stars: mass-loss — stars: winds — stars: Wolf-Rayet — X-rays: stars

## 1. Introduction

The *XMM-Newton* and *Chandra* observatories are now providing dramatic new high-resolution X-ray images and spectra of Wolf-Rayet (WR) stars. The improvements in sensitivity and spectral resolution offered by these observatories have effectively opened a new window for the study of WR winds and atmospheres. High-resolution spectra can potentially provide information on temperature structure, electron densities, chemical composition, and velocity profiles. A fundamental question that can now be addressed is the origin of the X-ray emission in WR stars, which has been a long-standing puzzle.

The most detailed X-ray studies of WR stars to date have focused on X-ray bright WR + OB binaries, for which high signal-to-noise spectra can be obtained in relatively short exposures. For example, high resolution *Chandra* and *XMM-Newton* grating spectra of  $\gamma^2$  Velorum (WC8 + O7.5) have recently been obtained (Skinner et al. 2001; Schmutz et al. 2002). In contrast, single WR stars without known companions are typically much fainter in X-rays and even moderate quality CCD spectra have been difficult to acquire. The capability to obtain CCD spectra of such fainter objects has now become available with *XMM-Newton*,

which provides the largest effective area ever achieved in an imaging X-ray telescope (Jansen et al. 2001). We present here the results of an *XMM-Newton* observation of the nitrogen-type WN 5-6 star WR 110 (= HD 165688), providing the best X-ray spectrum obtained so far of a WR star with no known companion.

Several unanswered questions motivate the study of X-ray emission from single WR stars. At a basic level, we would like to identify the physical process that is responsible for heating the plasma to X-ray emitting temperatures of several million K, and we would like to know if the same process is responsible for X-ray emission in both WR and OB stars. It is commonly assumed that the single WR and OB stars do emit X-rays by the same process and the emission is usually attributed to shocks that form in their powerful winds as a result of line-driven instabilities (Lucy & White 1980; Lucy 1982). The emergent X-ray emission is expected to be soft ( $kT \leq 0.5$  keV) and weakly absorbed. This mechanism has most generally been applied to OB stars, but radiative transfer models suggest that line-driven flow instabilities can also form in WR winds (Gayley & Owocki 1995).

Given the traditional belief that single WR and OB stars have a common X-ray emission mechanism, it is somewhat surprising that statistical X-ray correlations known to exist in OB stars are apparently not present in WR stars. Wesselowsky (1996) analyzed ROSAT data for a sample of 61 putatively single WN-type stars and found no evidence for the correlation between X-ray luminosity  $L_x$  and bolometric luminosity  $L_{bol}$  that is well-documented in single O-type stars (Berghöfer et al. 1997). Furthermore, no correlation between  $L_x$  and wind momentum loss rate  $\dot{M}v_\infty$  was seen in the WN star sample, in contrast to what might be expected if the X-rays arise in shocked winds. It is not yet known if these results reflect true differences between WR and OB star X-ray processes, or whether other factors such as undetected binarity might be responsible.

X-ray spectra of single WR stars are needed to address the basic question of the origin of their X-ray emission, and also to refine X-ray emission models of more complex WR + OB binaries. The X-ray emission of such binaries may be the superposition of intrinsic emission from the stars themselves plus an extrastellar component arising from colliding wind shocks between the two stars (Prilutskii & Usov 1976; Usov 1992). With the possible exception of WR 147 (Pittard et al. 2001), X-ray telescopes lack sufficient angular resolution to spatially resolve the stellar and colliding wind components. Thus, previous studies have assumed that the hot X-ray emission ( $kT \geq 1$  keV) detected in WR + OB spectroscopic binaries is due solely to colliding wind shocks, and that any intrinsic stellar contribution is negligible. Obviously this assumption needs to be tested by acquiring X-ray spectra of single WR and OB stars since a hot intrinsic stellar component (if present) could masquerade as colliding wind shock emission in spectroscopic binaries.

WR 110 is an ideal target for exploring the X-ray properties of single WR stars since it lies in an uncrowded field and there is no present evidence for binarity (Table 18 of van der Hucht 2001, hereafter vdH01). It also had the highest X-ray count rate of any single WR star detected by *ROSAT* ( $0.016 \text{ c s}^{-1}$  in a 8.3 ksec pointed observation, RP200717). Its visual magnitude is  $V = 9.4$  with moderate extinction  $A_V = 4.08$  mag and an estimated distance of 1.28 kpc (vdH01). The new XMM-Newton results presented here show that the X-ray emission of WR 110 is dominated by relatively cool plasma at  $kT_{cool} \approx 0.55 \text{ keV}$  ( $\approx 6 \text{ MK}$ ), but a hotter component is also present. We use the X-ray properties to place constraints on wind shock models and discuss possible origins of the hot component. In addition, we present the first multifrequency VLA observations of WR 110 which show that its radio properties are in good agreement with that expected for free-free emission from an ionized wind.

## 2. Observations

### 2.1. XMM-Newton Observations

*XMM-Newton* observed WR110 during a seven hour interval from 0147 - 0848 UT on 2001 March 22, yielding  $\approx 25$  ksec of usable exposure time (Table 1). The observatory consists of three X-ray telescopes as described by Jansen et al. (2001). Data were acquired with the European Photon Imaging Camera (EPIC) which provides simultaneous CCD imaging spectroscopy from the EPIC PN camera (Strüder et al. 2001) and two identical MOS cameras (MOS-1 and MOS-2; Turner et al. 2001). We utilized full-window mode and the medium optical blocking filter. Grating spectrometer data were also obtained but lacked sufficient counts for spectral analysis. The PN and MOS cameras provide a  $\approx 30'$  diameter field-of-view and energy coverage from  $\approx 0.2$  - 15 keV, moderate energy resolution ( $E/\Delta E \approx 20$  - 50), and  $\approx 12''$  FWHM angular resolution.

Data reduction followed standard procedures using the *XMM-Newton* Science Analysis System software (SAS vers. 5.1). The pipeline processing tasks EMCHAIN and EPCHAIN were executed using the latest calibration files and data were filtered with EVSELECT to select good event patterns. Spectra and light curves were extracted from the filtered events lists using circular regions of radius  $\approx 40''$ . Background was extracted from source-free regions of the same size on the same CCD as the source. Data from MOS-1 and MOS-2 were combined to increase the signal-to-noise ratio (S/N), thus reducing uncertainties in parameters derived from spectral fits and light curve analysis. Spectra were analyzed with XSPEC vers. 11 (Arnaud 1996) using a variety of models including discrete temperature

approximations (MEKAL, APEC) and differential emission measure (DEM) analysis. For the hard component, nonthermal power-law models were also examined. All models included an absorption component based on Morrison & McCammon (1983) cross sections.

## 2.2. VLA Observations

Radio observations of WR 110 were obtained with the NRAO <sup>2</sup> VLA in a three hour observation on 1999 Dec 26 with the array in B configuration, as summarized in Table 2. WR110 was observed and detected at four frequencies: 4.86 GHz (6 cm), 8.44 GHz (3.6 cm), 14.94 GHz (2 cm), and 22.46 GHz (1.3 cm). The star was observed with the full array at each frequency in scans of  $\approx$ 10 - 12 minutes duration interleaved with scans of the phase calibrator 1733–130. The primary flux calibrator 3C48 was observed at each frequency.

Data were edited and calibrated using the AIPS <sup>3</sup> software package. Maps were produced in both total intensity (Stokes *I*) and circularly polarized intensity (Stokes *V*) using the AIPS task IMAGR with natural weighting so as to maximize sensitivity. Both peak and total (integrated) fluxes were measured in cleaned maps using the AIPS tasks TVSTAT (pixel summation within a region defined by the  $2\sigma$  contour) and IMFIT (Gaussian source model). These two methods gave very good agreement, with typical differences of only 3% in the computed total flux.

## 3. Results

### 3.1. X-ray Properties of WR 110

#### 3.1.1. X-ray Images

Figure 1 shows the inner region of the EPIC-PN image within  $\approx$ 3 arc-min of WR110 in both broad-band (0.3 - 10 keV) and hard-band (6 - 10 keV) energy filters. WR 110 is clearly detected in both images. The X-ray position obtained by averaging the results of all three EPIC cameras (Table 1) is offset by only 0."/6 from the optical position (vdH01), providing high confidence that the X-ray source is associated with WR 110.

---

<sup>2</sup>The National Radio Astronomy Observatory (NRAO) is a facility of the National Science Foundation operated under cooperative agreement by Associated Universities Inc.

<sup>3</sup>Astronomical Image Processing System (AIPS) is a software package developed by NRAO.

The broad-band PN image yields 1916 raw counts from WR 110 in 22547 s, while MOS-1 gives 989 counts (25210 s) and MOS-2 gives 1034 counts (25207 s). The hard-band PN count rate is  $2.31 \pm 0.47 \text{ c ksec}^{-1}$  (6 - 10 keV) and the hard-band detection is confirmed in the combined MOS images. In addition, evidence for a hard component is seen in the spectra (Sec. 3.1.3). It is apparent from Figure 1 that the hard photons are localized at the WR 110 position and are not due to background. A second hard source lies  $52''$  NE of WR 110, but a SIMBAD search gives no counterpart within  $30''$  of the X-ray position of this second source.

### 3.1.2. X-ray Light Curves and Timing Analysis

Figure 2 shows the broad-band (0.3 - 10 keV) light curve of WR 110 obtained by combining data from the MOS-1 and MOS-2 detectors. The average count rate in the summed MOS light curve is  $0.084 \pm 0.013 (1\sigma) \text{ c s}^{-1}$ . A  $\chi^2$  test assuming a constant count-rate source gives a probability of constant count rate  $P(\text{const}) = 0.93$  ( $\chi^2/\text{dof} = 34.6/48$ ; binsize = 512 s, 49 bins). A smaller binsize of 256 s also gives  $P(\text{const}) = 0.93$  ( $\chi^2/\text{dof} = 77.7/97$ ; 98 bins). Thus there is no evidence for significant variability down to a binsize of 256 seconds. Various soft-band and hard-band light curves were also generated using larger binsizes of 2048 s to obtain an acceptable number of counts per bin, and a similar analysis showed no compelling evidence for variability.

The above results are consistent with the general behavior of hot stars, which rarely show X-ray variability on timescales of a few hours (e.g. Berghöfer et al. 1997). However, some WR + OB binaries which exhibit steady X-ray emission on short timescales are known to vary on orbital timescales of months to years (e.g. WR 11 and WR 140). Since long-term X-ray variability provides one possible means of detecting binarity, continued X-ray monitoring of WR 110 might be worthwhile (see also Sec. 4.4).

### 3.1.3. X-ray Spectra

The EPIC-PN spectrum shown in Figure 3 reveals prominent emission lines from the He-like ions Mg XI, Si XIII, and S XV. The spectrum also shows a rather narrow feature near 0.80 keV which we classify as a possible detection of Fe XVII and structure near 3.03 keV that is probably weak S XIV/XV emission. Using maximum line-power temperatures  $T_{\text{max}}$  as a guide (Mewe et al. 1985), we infer a range of plasma temperatures from  $\sim 6$  MK (Mg XI) up to at least  $\sim 16$  MK (S XV). It is thus obvious that the plasma is *not* isothermal

and our spectral analysis focuses on multi-temperature optically thin plasma models and DEM models.

Our attempts to derive abundances from the PN and MOS spectra show significant differences between the values inferred from VMEKAL and VAPEC optically thin plasma models. These differences occur even for elements with strong line emission such as Si and S, and we suspect that they are at least partially due to differences in atomic data used by the models. As such, reliable abundances for WR 110 cannot yet be determined from the CCD spectra. Thus, for purposes of spectral fitting, we adopted the typical WN abundances given in Table 1 of van der Hucht, Cassinelli, and Williams (1986, hereafter vdH86). These abundances reflect the chemical evolution that occurs in WN stars as a result of CNO-cycle burning, including hydrogen depletion and the enhancement of helium and nitrogen. Although the adopted abundances cannot be considered definitive, they do lie within the range of values reported in the literature for WN stars (Willis 1996). For comparison, we also give results for spectral fits using solar abundances (Anders & Grevesse 1989).

Discrete-temperature models with two temperature components (2T MEKAL and 2T APEC) converge rapidly to a cool component at  $kT_{cool} \approx 0.55$  keV and a hot component with an uncertain temperature. Similarly, DEM models show a dominant contribution from plasma at  $kT \approx 0.5$  keV as well as a turnup above 4 keV signalling hotter plasma. A representative DEM profile is shown in Figure 4, obtained from fits of the background-subtracted PN spectrum using the C6PVMKL model. This model uses an iterative algorithm based on Chebyshev polynomials (Lemen et al. 1989). As can be seen, the dominant component at  $kT \approx 0.5$  keV is a robust result and is recovered using canonical WN-star abundances as well as solar abundances. If the hot component is excluded, then the spectral fit is unacceptable above  $\sim 3$  keV as shown in the unfolded spectrum in Figure 5. These spectral analysis results, along with the clear detection of hard photons in the EPIC images, lead us to conclude that the hard emission is real and associated with WR 110.

Table 1 summarizes the plasma properties deduced from discrete-temperature and DEM models of the X-ray spectra using a single absorption component. These models give an equivalent neutral hydrogen column density  $N_H = 1.05 (\pm 0.18) \times 10^{22}$  cm $^{-2}$ . This value agrees to within the uncertainties with the value  $N_H = 0.91 (\pm 0.13) \times 10^{22}$  cm $^{-2}$  computed from the average visual extinction  $A_V = 4.08 \pm 0.58$  (Gorenstein 1975). This average  $A_V$  is slightly larger than that quoted in Table 24 of vdh01 since we have used a revised value  $A_V = 3.53$  from Schmutz & Vacca (1991) in computing the average. This revised value is based on the correct color excesses  $E_{b-v} = 0.86$  and  $E_{B-V} = 1.07$  (W. Schmutz, pers. comm.), rather than the misprinted values for WR 110 that appeared in Schmutz & Vacca (1991).

The temperature of the cool component is well-determined from both discrete-T and

DEM fits. This cool component is responsible for  $\approx 45\% - 55\%$  of the total observed (absorbed) flux in the 0.3 - 10 keV range and may account for as much as  $\approx 80\%$  of the intrinsic (unabsorbed) flux. The temperature of the hard component is considerably more uncertain. If the hard emission is thermal and subject to the same absorption as the cool component ( $N_H \approx 10^{22} \text{ cm}^{-2}$ ), then a temperature  $kT_{hot} \geq 3 \text{ keV}$  is required. Depending on the optically thin plasma model used, we obtain values in the range  $kT_{hot} \approx 3.5 - 8 \text{ keV}$ . Values of  $kT_{hot}$  somewhat below 3 keV may be possible if the hot component is more heavily absorbed, but fit statistics based on reduced  $\chi^2$  values do not favor such models.

A possibility worth considering is whether the hard X-ray component might be non-thermal emission. Hard X-rays with power-law spectra are predicted for such processes as inverse Compton scattering (Chen & White 1991), so we have compared models using an optically thin thermal plasma for both the cool and hot components with models which use a thin thermal plasma for the cool component and a power-law for the hot component. The reduced  $\chi^2$  values for these two cases are identical, with simultaneous fits of the PN spectrum and combined MOS spectra giving  $\chi^2_{red} = 0.89$  (96 dof) in both cases. The best fit photon power-law index is  $q = 2.2$  (1.9 - 2.6), where the parentheses enclose the 90% confidence range. Thus, we cannot rule out a power-law model for the hard X-ray emission based on the X-ray spectra alone and the issues concerning nonthermal X-ray emission are discussed further in Section 4.5.

### 3.2. Radio Properties

Figure 6 shows the 22 GHz VLA image with a clear detection of WR 110. The radio position (Table 2) is in excellent agreement with the SIMBAD optical position, with a radio – optical offset of  $\Delta\text{RA} = -0.0007$  s and  $\Delta\text{DEC} = +0.02''$ . As shown in Figure 7, the total flux  $S_\nu^{(total)}$  increases with frequency according to a power law  $S_\nu^{(total)} \propto \nu^\alpha$ , where  $\alpha = +0.64 \pm 0.10$  (90% confidence limits). This behavior is in excellent agreement with that expected for free-free emission from a spherical ionized constant-velocity wind (Wright & Barlow 1975). The total 4.86 GHz flux  $S_{4.86} = 1.17 \pm 0.04 \text{ mJy}$  (Table 2) is slightly larger than the value of  $0.96 \pm 0.10 \text{ mJy}$  measured with the VLA in C-configuration in July 1980 (Bieging, Abbott, & Churchwell 1982). The cleaned 4.86 GHz image shows no significant emission ( $\geq 4\sigma$ ) within  $30''$  of WR 110. Thus, there is no radio evidence of background AGNs near WR 110 that could contaminate the X-ray spectrum. No circular polarization is detected and the most stringent upper limit on fractional circular polarization ( $\pi_c$ ) comes from the 8.44 GHz Stokes V image. The rms noise in the 8.44 GHz Stokes V image is  $35 \mu\text{Jy}$ , giving a  $3\sigma$  upper limit  $\pi_c \leq 0.059$ .

The source is unresolved at the three lowest frequencies, as indicated by the good agreement between peak and total fluxes (Table 2). However, at the highest frequency of 22 GHz the peak flux is less than the total flux and the difference is significant ( $5.9\sigma$ ). This difference is present in the cleaned image obtained by combining *uv* data from all three 22 GHz scans ( $\approx 10$  minutes per scan) and also in the cleaned image of each scan. However, no significant difference is seen between the peak and total fluxes of the phase calibrator 1733–310. These results raise the interesting possibility that the radio source is partially resolved at 22 GHz with a synthesized beam of  $0.^{\prime\prime}6 \times 0.^{\prime\prime}3$ . Using the current best estimates for the mass-loss parameters given below (Sec. 3.2.1), the effective 22 GHz angular size of the radio emitting region of an ideal spherical wind is  $<0.^{\prime\prime}02$  at  $d = 1.28$  kpc (Panagia & Felli 1975). If the adopted distance is correct, then it is unlikely that the VLA is resolving the wind unless it is highly non-spherical. An alternate explanation is that two or more radio-emitting components lie within the synthesized beam. To be marginally resolved at 22 GHz, the angular separation between components would need to be at least  $\approx 0.^{\prime\prime}3$ , which equates to a projected linear separation of at least  $\sim 384$  AU at  $d = 1.28$  kpc. Given that the present evidence for partially resolved radio emission is based on limited high-frequency 22 GHz snapshot data, we believe that confirmation will be necessary in higher angular resolution observations with more complete *uv* coverage.

### 3.2.1. Mass Loss Rate

The ionized mass loss rate for an assumed constant-velocity wind can be estimated using the result of Wright & Barlow (1975), namely  $\dot{M} = C_0 v_\infty S_\nu^{0.75} d^{1.5} M_\odot \text{ yr}^{-1}$ , where  $C_0 = 0.095\mu/[Z\sqrt{\gamma g\nu}]$ . Here,  $v_\infty$  ( $\text{km s}^{-1}$ ) is the terminal wind speed,  $S_\nu$  ( $\text{Jy}$ ) is the observed radio flux at frequency  $\nu$  ( $\text{Hz}$ ),  $d$  ( $\text{kpc}$ ) is the stellar distance,  $\mu$  is the mean atomic weight per nucleon,  $Z$  is the rms ionic charge,  $\gamma$  is the mean number of free electrons per nucleon, and  $g$  is the free-free Gaunt factor. To evaluate this expression we use the highest signal-to-noise radio detection at  $\nu = 8.44$  GHz,  $S_{8.44} = 1.77$  mJy (Table 2),  $v_\infty = 2100 \text{ km s}^{-1}$  (vdH01),  $d = 1.28$  kpc (vdH01),  $Z = 1$  (vdH86),  $\gamma = 0.96$  (vdH86), and  $g = 4.78$  at 8.44 GHz from the approximation for the free-free Gaunt factor given in Eq. [8] of Abbott et al. (1986), assuming a temperature at the radio photosphere of  $T = 10000$  K (vdH86). These values give  $\dot{M} = 1.267\mu \times 10^{-5} M_\odot \text{ yr}^{-1}$ . Assuming  $\mu = 3.9$  for a WN star (vdH86), one obtains  $\dot{M} = 4.9 \times 10^{-5} M_\odot \text{ yr}^{-1}$ . This mass-loss rate gives a wind luminosity  $L_{wind} = (1/2)\dot{M}v_\infty^2 = 6.8 \times 10^{37} \text{ ergs s}^{-1}$ .

### 3.3. Filling Factor of X-ray Emitting Gas

An important quantity for constraining X-ray emission models is the average filling factor  $f$  which is defined by the ratio  $f = \text{EM}_x/\text{EM}_{tot}$ . Here,  $\text{EM}_x$  is the volume emission measure of the X-ray emitting plasma and  $\text{EM}_{tot}$  is the total volume emission measure of the wind. For radiative shock models, the value of  $f$  provides a rough measure of the fraction of the wind that is undergoing instability developments and  $f$  is also useful in comparing the X-ray properties of WR and O-type stars (Ignace, Oskinova, & Foullon 2000). One advantage of obtaining both X-ray and radio data is that  $f$  can be calculated in a straightforward manner.

$\text{EM}_x$  is obtained from X-ray spectral fits via the XSPEC normalization parameter *norm* in MEKAL and VMEKAL models, which is defined by  $\int n_e n_H dV = 10^{14} (4\pi d^2) \cdot \text{norm} \text{ cm}^{-3}$ . Using  $d = 1.28$  kpc and the adopted canonical WN abundances with  $n_{He} = 14.9 n_H$  (vdH86), we obtain the X-ray emission measure of a helium-dominated plasma  $\text{EM}_x = 3.12 \times 10^{59} \cdot \text{norm} \text{ cm}^{-3}$ . For an assumed constant-velocity spherical wind,  $\text{EM}_{tot}$  is related to the observed radio flux via the relation given in Eq. [7] of Abbott et al. (1986). Inserting the 8.44 GHz parameters given above (Sec. 3.2.1) into Eq. [7] of Abbott et al. we obtain  $\text{EM}_{tot} = 5.5 \times 10^{60} \mathcal{I} (R_*/R_\odot)^{-1} \text{ cm}^{-3}$ , where  $\mathcal{I} = \int w^{-2} dx$  is the dimensionless wind-velocity integral that enters into the calculation. The variable of integration is  $x = R_*/r$  where  $w = v/v_\infty = 1$  and  $\mathcal{I} = 1$  for a spherical constant-velocity wind. We adopt the value  $\mathcal{I} = 14$  appropriate for the wind velocity law of Abbott et al. and thereby obtain  $f = 4.05 \times 10^{-3} \cdot \text{norm} (R_*/R_\odot)$ .

The stellar radius is uncertain, but values in the range  $R_* = 1.8 - 6 R_\odot$  have been estimated in previous work (Abbott et al. 1986; Hamann et al. 1995). The XSPEC *norm* value is also uncertain since it depends on the abundances used to fit the X-ray spectrum. If the spectrum is fitted with a 2T MEKAL model using canonical WN abundances (vdH86) then  $\text{norm} = \text{norm}_1 + \text{norm}_2 = (1.25 + 0.50) \times 10^{-5}$ , where  $\text{norm}_1$  and  $\text{norm}_2$  correspond to the cool ( $kT_{cool} = 0.55$  keV) and hot ( $kT_{hot} \geq 3$  keV) components. Allowing for the uncertainty in  $R_*$  we obtain  $f = (1.3 - 4.1) \times 10^{-7}$ , or an order-of-magnitude estimate  $f \sim 10^{-7}$ . The above range in  $f$  includes the contributions of both the cool and hot plasma components. If only the cool component is included, then  $f$  decreases by  $\approx 28\%$  but the order-of-magnitude result is unchanged. The same 2T MEKAL model using solar abundances gives slightly larger values  $f = (0.66 - 2.1) \times 10^{-6}$  or  $f \sim 10^{-6}$ , including contributions from both the cool and hot components.

## 4. Discussion

The new XMM results discussed above reveal a two-component X-ray structure for WR 110, consisting of both soft and hard X-ray emission. We discuss possible emission mechanisms below. The leading model for explaining the soft emission is based on the instability-driven wind-shock picture (Sec. 4.1), while several alternative mechanisms are examined for explaining the hard emission (Secs. 4.2 - 4.5).

### 4.1. Instability-Driven Wind Shocks

The instability-driven wind shock model attributes the the X-ray emission from single hot stars to shocks that are distributed throughout the wind (Lucy & White 1980; Lucy 1982; Owocki et al. 1988; Feldmeier et al. 1997). Some observational support for this model has now been obtained in X-ray grating spectra of the O4 supergiant  $\zeta$  Puppis (Cassinelli et al. 2001; Kahn et al. 2001). The stronger emission lines in the  $\zeta$  Pup spectrum such as Ne X are blueshifted, consistent with predictions for line formation in an outflowing wind (e.g. Owocki & Cohen 2001). However, grating observations have so far failed to detect such Doppler shifts in other putatively single O-type stars (e.g. Schulz et al. 2000; Waldron & Cassinelli 2001) or in the X-ray bright WC8 + O7 binary  $\gamma^2$  Vel (Skinner et al. 2001). Additional X-ray grating observations of a larger sample of hot stars are clearly needed to confirm the presence of Doppler shifts. Another potential problem is that the instability-driven shock model has difficulties accounting for the S XV line in the  $\zeta$  Pup spectrum, which apparently forms near the base of the wind where post-shock velocities (and the corresponding shock temperatures) are expected to be low.

The XMM-Newton data for WR 110 present a new challenge for the instability-driven wind shock model, which predicts only soft X-rays. Although this model might be able to explain the cool emission component in WR 110, the hot emission component is not predicted by current versions of this model and will thus require a different explanation (Secs. 4.2 - 4.5). Assuming that the cool emission is due to instability-driven wind shocks, we can place constraints on the range of shock velocities present and can also estimate the minimum radius from which the detected X-rays emerge.

To estimate the range of shock velocities needed to account for the cool component, we use the relation for the post-shock temperature of a strong adiabatic shock is  $kT_s = (3/16)\bar{m}v_s^2$ , where  $\bar{m}$  is the mean particle mass in the wind and  $v_s$  is the shock velocity. For a helium-rich WN wind we have  $\bar{m} = (4/3)m_p$  where  $m_p$  is the proton mass. The observed temperature  $kT_{cool} = 0.55$  keV gives a typical shock velocity  $v_s = 460$  km s<sup>-1</sup>.

However, the DEM distribution (Fig. 4) spans a range of temperatures from  $kT_{cool} \approx 0.3$  - 0.8 keV (FWHM), so the observations imply a range of shock velocities from 340 - 550 km s<sup>-1</sup>. These values are about a factor of two larger than predicted using the original radiative-shock formulation of Lucy (1982).

To estimate the minimum radius from which the detected X-rays emerge, we assume that the wind is spherical and homogeneous. In that case, the emergent X-rays detected in our observation must come from radii larger than the radius  $R_{\tau=1}(E)$  at which the wind becomes optically thin. Although X-rays could be produced at smaller radii, they would have escaped detection due to absorption by the overlying wind. Using the mass-loss parameters in Sec. 3.2.1 and the WN wind cross-sections  $\sigma_w$  for X-rays from Ignace et al. (2000), we obtain  $R_{\tau=1}(E = 1 \text{ keV}) = 1.8 \times 10^{14} \text{ cm} \approx 12 \text{ AU}$ . For an assumed stellar radius  $R_* = 4 R_\odot$ , this equates to  $R_{\tau=1}(E = 1 \text{ keV}) = 645 R_*$ . By comparison, the wind absorption cross-sections are much lower at high energies with an approximate dependence  $\sigma_w \propto E^{-2.5}$  (Fig. 1 of Ignace et al. 2000), and the hard component emission detected above  $\sim 3$  keV could thus originate at radii of less than  $\sim 1$  AU.

If stellar X-rays suffered significant absorption by circumstellar material, in addition to wind absorption, then the above calculation would underestimate  $R_{\tau=1}(E)$ . However, there is no reason to believe that significant circumstellar X-ray absorption has occurred for WR 110. The value of  $N_H$  determined from the X-ray spectra is consistent with that inferred from the visual extinction (Sec. 3.1.3), so the emergent X-rays have not incurred any significant excess absorption above that seen in the optical. There is no evidence for H or circumstellar material in the optical spectra (Schmutz, Hamann, & Wesselowsky 1989). For circumstellar material to have escaped optical detection, it would have to be largely unionized which would be unlikely given the high stellar effective temperature (Hamann et al. 1995). We thus believe that the neutral hydrogen column density  $N_H = 1.05 \times 10^{22} \text{ cm}^{-2}$  is due mainly to interstellar absorption, which is expected to be large for WR 110 since it is viewed toward the galactic center (galactic coordinates  $l = 10.8$ ,  $b = +0.39$ ).

Thus, for an ideal spherical homogeneous wind we conclude that the emergent cool X-ray emission comes from hundreds of stellar radii whereas the harder emission could originate much closer to the star. If the wind is aspherical or inhomogeneous (e.g. clumpy) then  $R_{\tau=1}(E)$  depends on geometry and clump properties. In that case, even the cool emission detected in our observation could come from smaller radii than estimated above.

#### 4.2. Magnetically-Confining Wind Shocks

The detection of a hard emission component in WR 110 is of interest given that hot plasma has also been reported in O-type stars such as  $\theta^1$  Ori C (Schulz et al. 2000) and  $\zeta$  Ori (Waldron & Cassinelli 2001). The traditional view that hot stars emit only soft weakly-absorbed X-rays is now being replaced by a more complex picture that also requires high-temperature plasma originating close to the star. It has been suggested that the hot plasma may be magnetically confined near the base of the wind and this has sparked renewed interest in magnetically-confined wind shock models. Such models were originally proposed to explain the X-ray emission of magnetic Ap-Bp stars (Babel & Montmerle 1997a) but were subsequently extended to young O-type stars such as  $\theta^1$  Ori C (Babel & Montmerle 1997b).

In this picture the ionized wind is trapped by a (dipolar) magnetic field and is then channeled along field lines toward the magnetic equatorial plane where the two streams from the separate hemispheres collide to produce an X-ray emitting shock. A dense geometrically thin cooling disk is predicted to form in the equatorial plane. This process is capable of producing high-temperature plasma and thus might be considered as a means of explaining the hard emission component in WR 110.

At present, it seems quite difficult to justify the above model for WR stars in general, and for WR 110 in particular. There is, to our knowledge, no persuasive evidence for magnetic activity in WR 110. This contrasts with O-type stars such as  $\theta^1$  Ori C which show clear rotational modulation in X-rays and H $\alpha$ . However, additional searches for evidence of magnetic fields would be valuable since magnetically-active regions have been proposed as a possible explanation of the 3.766 d optical and ultraviolet periodicity detected in the WN 4 star EZ CMa (St.-Louis et al. 1995). Although previous observations suggest that the X-ray emission of EZ CMa is variable, there is no evidence so far that the X-rays are modulated at the 3.766 d optical period (Willis & Stevens 1996; Skinner, Itoh, & Nagase 1998).

Another potential difficulty is that WR stars typically have much larger mass-loss rates than O-type or Ap-Bp stars and proportionally larger magnetic fields are required for wind confinement. The degree to which the wind is confined by the magnetic field is determined by the confinement parameter  $\Gamma = B_0^2 R_*^2 / \dot{M} v_\infty$ , where  $B_0$  is the surface equatorial field strength (ud-Doula & Owocki 2002). If  $\Gamma \gg 1$  then the wind is strongly confined but if  $\Gamma \ll 1$  then the field is stretched out by the wind. Assuming  $R_* = 4 R_\odot$  for WR 110 and using the adopted mass-loss parameters (Sec. 3.2.1) gives  $B_0 = 2.9 \sqrt{\Gamma}$  kG. Thus, surface fields of several kG are required for confinement. Electrons trapped in such a strong field should emit nonthermal radio emission as recognized by Babel & Montmerle (1997a), but such emission could be masked by heavy wind absorption in WR stars.

Magnetic fields of several kG would also imply much higher X-ray luminosities from a magnetically-confined wind shock than derived from the XMM spectra. The predicted luminosity for a marginally confined wind in WR 110 using  $B_0 = 2.9$  kG is at least  $L_x \approx 10^{36.6}$  ergs s $^{-1}$  (eq. [10] of Babel & Montmerle 1997a). This value is four orders of magnitude larger than observed, which is a large mismatch. We also note that very efficient conversion of wind kinetic energy to thermal X-rays was required for this model to successfully explain the X-ray emission of the Ap star IQ Aur (Babel & Montmerle 1997a). In contrast, the mechanism responsible for the X-ray emission in WR 110 is very inefficient since  $L_x/L_{wind} \sim 10^{-5}$ .

Thus, in its current form, there are several difficulties that need to be addressed in order to extrapolate the magnetically-confined wind shock model to WR stars. Obviously, persuasive evidence for magnetic activity is the main missing link and further observational work is needed to search for periodic variability in emission lines and the continuum at all wavelengths (including X-rays) as well as nonthermal radio emission. Further extensions of the theory are also needed to test it in the high mass-loss WR regime. The distortion of the magnetic field by the wind is of particular importance in the case of WR stars, and the effects of dipole magnetic fields on line-driven outflows have been incorporated into recent numerical magnetohydrodynamic simulations (ud-Doula & Owocki 2002).

### 4.3. Wind Accretion Shocks

Given the potential difficulties with magnetic wind shock models for WR stars, we consider other alternatives for explaining the hard X-ray emission. It is conceivable that the hard X-rays are due either to gravitational accretion of the WR wind onto an optically faint companion which has so far escaped detection, or to the WR wind shocking onto such a companion.

Gravitational accretion onto an optically faint neutron star companion is one possibility that is consistent with evolutionary scenarios for massive binaries (van den Heuvel 1976). However, the expected X-ray luminosity from accretion of the WR wind onto a neutron star is much larger than observed and we believe this option is unlikely. Specifically, for an assumed neutron star mass  $M_{ns} = 1.4 M_\odot$  and  $M_{WR} = 7.7 M_\odot$  (Hamann et al. 1995), the results of Davidson & Ostriker (1973) give a predicted unabsorbed accretion luminosity of at least  $L_{x,acc} \sim 10^{37}$  ergs s $^{-1}$ . This value is several orders of magnitude larger than the intrinsic luminosity of WR 110 obtained from spectral fits (Table 1).

Gravitational accretion onto a faint normal (nondegenerate) stellar companion is also

possible, but again seems unlikely. The gravitational radius is  $R_G = 2GM_{comp}/v_w^2$  where  $G$  is the gravitational constant,  $M_{comp}$  is the mass of the putative companion, and  $v_w$  is the WR wind velocity. Using  $v_w = 2100 \text{ km s}^{-1}$  gives  $R_G/R_\odot = 0.38 (M_{comp}/M_\odot)/v_{1000}^2$ , where  $v_{1000}$  is the WR wind velocity in units of  $1000 \text{ km s}^{-1}$ . Assuming a solar-like companion with  $M_{comp} \approx M_\odot$  and  $R_{comp} \approx R_\odot$  we obtain  $R_G = 0.09 R_\odot$ . Thus,  $R_G \ll R_{comp}$  and gravitational accretion is ineffective. We thus consider the more likely case below in which the WR wind collides directly with the surface of the putative companion.

#### 4.4. Colliding Wind Shocks

Although the temperature of the hot component is not tightly constrained, spectral fits with optically thin plasma models are consistent with values as high as  $kT_{hot} \approx 8 \text{ keV}$ . Such high temperatures could be produced if the WR wind overwhelms that of a lesser companion, forming an adiabatic shock at or near the companion surface. In that case the temperature relation for a strong adiabatic shock gives  $kT_s = (3/16)\bar{m}v_s^2 \approx 11 \text{ keV}$ , where we have assumed that the WR wind has reached terminal speed and thus  $v_s \approx v_\infty = 2100 \text{ km s}^{-1}$ . Assuming that the hot plasma detected in WR 110 is free-free emission from such an adiabatic shock, we can place constraints on the companion separation  $a$  using two different approaches based on timescales and X-ray luminosity.

The relevant dynamical timescale is  $t_d = a/v_\infty$ , where  $v_\infty$  is the terminal speed of the WR wind. If the high-temperature plasma is free-free emission from a strong adiabatic shock at (or near) the companion surface, then the cooling time  $t_{cool}$  of the plasma behind the shock must be greater than  $t_d$  while the opposite is true for the electron-ion equilibration time  $t_{ei}$ . Thus  $t_{ei} < t_d < t_{cool}$ .

In the case of a pure helium wind we can write  $t_{ei} = 8.38 T_s^{3/2} n_{He}^{-1}$  (Spitzer 1962) and  $t_{cool} = (3/2) (n_{He} + n_e) kT_s \epsilon_{ff}^{-1} = 5.41 \times 10^{10} T_s^{1/2} n_{He}^{-1}$ . Here, we have used the explicit expression for free-free emissivity  $\epsilon_{ff}$  from Allen (1973) assuming a Gaunt factor of unity. Using the standard expressions for the post-shock number density  $n_{He}$  and temperature  $T_s$  and the assumption of a spherical wind, the above inequality becomes  $0.68 \dot{M}_5 v_{1000}^{-3} < a_{AU} < 144.6 \dot{M}_5 v_{1000}^{-5}$ , where  $\dot{M}_5$  is the WR mass loss rate in units of  $10^{-5} M_\odot \text{ yr}^{-1}$ ,  $v_{1000}$  is the terminal wind velocity in units of  $1000 \text{ km s}^{-1}$ , and  $a_{AU}$  is the companion separation in AU. Substituting the WR 110 mass-loss parameters (Sec. 3.2.1) gives  $0.36 < a_{AU} < 17.3$ .

A more stringent constraint on  $a$  is obtained by equating the intrinsic X-ray luminosity of the hard component with the adiabatic shock luminosity  $L_{x,s}$ . The intrinsic (unabsorbed) flux of the hot component determined from the thermal thin plasma models of the X-ray

spectra is  $F_{x,hot}(0.3 - 10 \text{ keV}) = 4 \times 10^{-13} \text{ ergs cm}^{-2}$ , which gives  $L_{x,s} = 7.8 \times 10^{31} \text{ ergs s}^{-1}$ . This value is of course a lower limit since our flux measurement is restricted to a specific energy range. We assume that the strong WR wind overwhelms that of the faint companion, in which case the companion can be approximated by a hard sphere. Inserting the above value of  $L_{x,s}$  and the WR 110 mass-loss parameters into eq. [81] of Usov (1992) gives  $a_{AU} = 0.28(R_{comp}/R_{\odot})^{0.75}$ .

If  $R_{comp} = 1.4 R_{\odot}$  then the above luminosity constraint gives  $a = 0.36 \text{ AU}$ , which is consistent with the lower limit derived from the timescale argument. If the putative companion were a main-sequence star then the minimum radius  $R_{comp} = 1.4 R_{\odot}$  would correspond to a late A spectral type. However, there is considerable leeway in the spectral type since the luminosity class is unknown and larger values of  $R_{comp}$  are required if  $a > 0.36 \text{ AU}$ . At the minimum separation  $a = 0.36 \text{ AU}$ , some absorption of the hard X-rays could occur, but as noted above the amount of absorption will depend on the symmetry and homogeneity properties of the wind.

#### 4.5. Nonthermal X-ray Emission

As noted in Sec. 3.1.3, we cannot formally rule out a power-law model for the hard X-ray emission based on X-ray spectral fits alone. We thus comment briefly on nonthermal emission models. In the model proposed by Chen & White (1991, hereafter CW91), hard X-ray photons can be produced in hot stars by inverse Compton scattering of stellar UV photons off of relativistic shock-accelerated particles in the wind. This model was applied to OB supergiants by CW91 but it may have broader relevance to all hot stars that are subject to line-driven instabilities. However, bremsstrahlung may be as important as inverse Compton scattering in dense WR winds (CW91).

The inverse Compton model makes some predictions that can be compared with observations. The X-rays are not expected to show large amplitude variations and this is consistent with the temporal behavior of WR 110, at least for the relatively short seven hour observation analyzed here. The predicted photon power-law index in the hard X-ray band is  $q = 1.5$ , whereas the value inferred from the EPIC spectra for WR 110 is  $q = 2.2$  (1.9 - 2.6). Given the relatively low signal-to-noise ratio in the EPIC spectra above  $\sim 3 \text{ keV}$ , this difference may not be problematic. The model also provides an expression for evaluating the hard-band X-ray luminosity but it is quite sensitive to the assumed wind temperature and mass-loss parameters (eqs. [31] - [32] of CW91). Evaluation of the expression for the hard-band luminosity also requires a value for the stellar magnetic field strength, which is not known for WR 110 or for WR stars in general.

The hard X-rays from inverse Compton scattering in the CW91 model are predicted to originate within  $10 R_*$  of the star where the stellar UV photon number density is high. This is a potential problem for WR stars since their winds could be optically thick even to harder X-rays of several keV this close to the star (Sec. 4.1). However, this problem is mitigated if the wind is clumped.

The inverse Compton model does not predict a coincidence between nonthermal X-rays and nonthermal radio emission. Thus, the absence of nonthermal radio signatures in WR 110 is not necessarily in conflict with an inverse Compton origin for the hard X-rays. If radio synchrotron emission is formed within the wind (White 1985), it could be absorbed. Using the adopted mass-loss parameters for WR 110, we estimate  $R_{\tau=1} \approx 3380 R_\odot$  at  $\nu = 8.44$  GHz, or  $R_{\tau=1} \approx 845 R_*$  assuming  $R_* \approx 4 R_\odot$ . Thus, nonthermal radio emission formed even at hundreds of stellar radii could escape detection.

Although an interpretation of the hard X-rays in terms of the inverse Compton model does not appear to conflict with our data, there are some concerns about the relevance of this model to WR 110. Without specific knowledge of wind clumping properties, it is not clear that hard X-rays ( $kT \geq 3$  keV) produced within  $\sim 10 R_*$  would penetrate the dense overlying wind and be detected. Furthermore, direct evidence for relativistic particles in the wind is lacking since the VLA data show no obvious signs of nonthermal radio emission (e.g. synchrotron emission). To our knowledge, there have been no confirmed detections of non-thermal X-ray emission in any WR star to date. However, hard *thermal* X-rays accompanied by Fe K emission lines have been detected in some well-studied WR + OB binaries such as WR 140 (Koyama et al. 1994) and  $\gamma^2$  Vel (Skinner et al. 2001). Considering the above factors, we believe that the hard X-rays in WR 110 are more likely to be of thermal origin rather than nonthermal.

## 5. Summary and Outlook

XMM-Newton provides the largest effective area ever achieved in an imaging X-ray telescope and we have utilized this new capability to obtain the first high-quality X-ray spectrum of a Wolf-Rayet star with no known companion (WR 110). We have also acquired the first multifrequency radio observations of WR 110 which clearly show that its spectral energy distribution is in good agreement with that expected for free-free wind emission.

The new X-ray data yield some surprises and raise several new questions about the origin of X-ray emission in WR stars. We have shown that the X-ray emission is dominated by a cool component with a characteristic temperature  $kT_{cool} \approx 0.5$  keV ( $\approx 6$  MK), but that

a hard component is also present. The presence of hard emission is not anticipated on the basis of current instability-driven wind shock models for single hot stars, and we have argued that the hard emission could be due to the WR wind shocking onto an as yet undetected close companion. However, until compelling evidence for binarity is found we cannot exclude the possibility that the hard emission is intrinsic to WR 110.

Further observational and numerical work will be needed to address the following issues:

1. Numerical simulations of instability-driven wind shocks in WR stars are needed to produce synthetic spectra that can be directly compared with recent X-ray observations. One question to be addressed is whether instability-driven shocks can account for higher temperature spectral lines such as S XV ( $T_{max} \sim 16$  MK) that are seen in WR 110 and in other putatively single O-type stars such as  $\zeta$  Pup and  $\zeta$  Ori. Such simulations will also need to determine if radiative shocks can persist to hundreds of stellar radii in WR winds, in analogy with studies for O-type stars recently undertaken by Runacres & Owocki (2002). If not, then a clumped wind may be needed to reconcile the cool emission detected in WR 110 with the conventional wind shock picture.
2. Further observational work is needed to determine if the hard X-ray emission detected in WR 110 is a common feature of “single” WR stars, or an anomaly. Good-quality X-ray spectra of a larger sample of putatively single WR stars are needed to answer this question.
3. Further searches for evidence of binarity in WR 110 and other X-ray emitting “single” WR stars are needed. We have argued that a close stellar companion could explain the hard emission in WR 110, and binarity is a good bet since 38% of presently catalogued WR stars are *known* binaries (vdH01). Given the difficulty of detecting faint companions around high-luminosity WR stars ( $L_{bol} \sim 10^5 L_{\odot}$ ), the true binary fraction is undoubtedly higher. If close companions are ultimately detected around X-ray emitting WR stars that are now thought to be single, then legitimate single WR stars may turn out to be much fainter in X-rays than currently believed.
4. If sensitive searches for binarity in “single” WR stars yield negative results, then the instability-driven wind shock paradigm may need to be revised. Further work on magnetically-confined wind shock models is needed to assess their relevance to WR stars in the high mass-loss regime where the wind stretches out the field. Additional hard X-ray and  $\gamma$ -ray observations of WR stars should also be undertaken to search for high-energy emission in the MeV to GeV range that could arise from nonthermal processes such as inverse Compton scattering.

This work was supported by NASA grant NAG5-10362. SZh acknowledges the support of NASA grant NAG5-8236. Research at PSI is supported by grant 2100-049343 from the Swiss NSF. This work was based on observations obtained with XMM-Newton, an ESA science mission with instruments and contributions directly funded by ESA member states and the USA (NASA). We thank members of the XMM-Newton, VLA, and HEASARC (NASA/GSFC) support teams for their assistance. This research has made use of the SIMBAD astronomical database operated by CDS at Strasbourg, France.

Table 1. X-ray Properties of WR110<sup>a</sup>

Parameter	Value
PN Count Rate (c s <sup>-1</sup> )	0.085
MOS Count Rate (c s <sup>-1</sup> )	0.039 (M1), 0.041 (M2)
N <sub>H</sub> (10 <sup>22</sup> cm <sup>-2</sup> )	1.05 ± 0.18
kT (keV)	0.55 ± 0.07 + hot
Flux (10 <sup>-12</sup> ergs cm <sup>-2</sup> s <sup>-1</sup> )	0.37 (2.1)
L <sub>x</sub> (10 <sup>32</sup> ergs s <sup>-1</sup> )	0.72 (4.1)

<sup>a</sup>The X-ray position obtained by averaging the results of all three EPIC cameras is RA(2000) = 18 h 07 m 56.95 s, DEC(2000) =  $-19^\circ 23' 57.4''$ . The column density (N<sub>H</sub>) and X-ray temperature (kT) were derived from best-fit single-absorber MEKAL and C6PVMKL models using the canonical WN abundances given in vdH86. The temperature of the hot component is uncertain, but if N<sub>H</sub> is the same for the hot and cool components then kT<sub>hot</sub>  $\geq$  3 keV. Flux and L<sub>x</sub> are the observed (absorbed) values in the 0.3 - 10 keV range, followed in parentheses by intrinsic (unabsorbed) values. A distance of 1.28 kpc is assumed.

Table 2. VLA Observations of WR110<sup>a</sup>

Frequency (GHz)	Beam FWHM (arcsec)	Duration (min.)	RMS Noise ( $\mu$ Jy/beam)	Peak Flux (mJy/beam)	Total Flux (mJy)
4.86	$2.9 \times 1.4$	23	41	1.22	1.17
8.44	$1.5 \times 0.8$	22	35	1.77	1.77
14.94	$0.8 \times 0.4$	31	100	2.44	2.46
22.46	$0.6 \times 0.3$	31	150	2.20	3.09

<sup>a</sup>All data were obtained in B configuration on 1999 Dec 26 from 1855 - 2152 UT. Observations were obtained at each frequency in two orthogonal polarization channels, each with a bandwidth of 50 MHz. Fluxes and beam sizes are from cleaned Stokes I maps. Primary flux calibrator was 3C48. The radio position of WR110 measured from 8.44 GHz maps is RA(2000) = 18 h 07 m 56.959 s, DEC(2000) =  $-19^\circ 23' 56.85''$ .

## REFERENCES

- Abbott, D.C., Bieging, J.H., Churchwell, E., & Torres, A.V. 1986, *ApJ*, 303, 239
- Allen, C.W. 1973, *Astrophysical Quantities* (Athlone Press)
- Anders, E., & Grevesse, N. 1989, *Geochim. Cosmochim. Acta*, 53, 197
- Arnaud, K.A. 1996, in *Astronomical Data Analysis Software and Systems V*, eds. G. Jacoby & J. Barnes, (San Francisco: ASP), 101, 17
- Babel, J. & Montmerle, T., 1997a, *A&A*, 323, 121
- Babel, J. & Montmerle, T., 1997b, *ApJ*, 485, L29
- Berghöfer, T.W., Schmitt, J.H.M.M., Danner, R., & Cassinelli, J.P., 1997, *A&A*, 322, 167
- Bieging, J.H., Abbott, D.C., & Churchwell, E.B., 1982, *ApJ*, 263, 207
- Cassinelli, J.P., Miller, N.A., Waldron, W.A., MacFarlane, J.J., & Cohen, D.H., 2001, *ApJ*, 554, L55
- Chen, W. & White, R.L., 1991, *ApJ*, 366, 512 (CW91)
- Davidson, K. & Ostriker, J.P., 1973, *ApJ*, 179, 585
- Dulk, G.A., 1985, *ARA&A*, 23, 169
- Feldmeier, A., Kudritzki, R.-P., Palsa, R. Pauldrach, A.W.A., & Puls, J., 1997, *A&A*, 320, 899
- Gayley, K.G. & Owocki, S.P., 1995, *ApJ*, 446, 801
- Gorenstein, P. 1975, *ApJ*, 198, 95
- Hamann, W.-R., Koesterke, L., & Wessolowski, U., 1995, *A&A*, 299, 151
- Ignace, R., Osokinova, L.M., & Foullon, C., 2000, *MNRAS*, 318, 214
- Jansen, F. et al., 2001, *A&A*, 365, L1
- Kahn, S.M. et al., 2001, *A&A*, 365, L312
- Koyama, K., Maeda, Y., Tsuru, T., Nagase, F., & Skinner, S., 1994, *PASJ*, 46, L93
- Lemen, J.R., Mewe, R., Schrijver, C.J., & Fludra, A., 1989, *ApJ*, 341, 484

- Lucy, L.B., 1982, *ApJ*, 255, 286
- Lucy, L.B. & White, R.L., 1980, *ApJ*, 241, 300
- Luo, D., McCray, R., & MacLow, M-M., 1990, *ApJ*, 362, 267
- Mewe, R., Gronenschild, E.H.B.M., & van den Oord, G.H.J., 1985, *A&AS*, 62, 197
- Morrison, R. & McCammon, D. 1983, *ApJ*, 270, 119
- Owocki, S.P., Castor, J.I., & Rybicki, G.B., 1988, *ApJ*, 335, 914
- Owocki, S.P. & Cohen, D.H. 2001, *ApJ*, 559, 1108
- Panagia, N. & Felli, M., 1975, *A&A*, 39, 1
- Pittard, J.M. et al., 2001, *A&A*, submitted
- Prilutskii, O., Usov, V.V., 1976, *SvA-AJ*, 20,2
- Runacres, M.C. & Owocki, S.P., 2002, *A&A*, 381, 1015
- Schmutz, W., Hamann, W.-R., & Wesselowski, U., 1989, *A&A*, 210, 236
- Schmutz, W. & Vacca, W.D., 1991, *A&AS*, 89, 259
- Schmutz, W. et al., 2002, in *New Visions of the X-ray Universe*, in prep.
- Schulz, N.S., Canizares, C.R., Huenemoerder, D., & Lee, J.C., 2000, *ApJ*, 545, L135
- Skinner, S.L., Güdel, M., Schmutz, W., & Stevens, I.R., 2001, *ApJ*, 558, L113
- Skinner, S.L., Itoh, M., & Nagase, F. 1998, *New Astron.*, 3, 37
- Spitzer, L., 1962, *Physics of Fully Ionized Gases* (New York: J. Wiley)
- St.-Louis, N., Dalton, M.J., Marchenko, S.V., Moffat, A.F.J., & Willis, A.J., 1995, *ApJ*, 452, L57
- Strüder, L. et al., 2001, *A&A*, 365, L18
- Turner, M.J.L. et al., 2001, *A&A*, 365, L27
- ud-Doula, A. & Owocki, S.P., 2002, *ApJ*, submitted
- Usov, V.V. 1992, *ApJ*, 389, 635

- van den Heuvel, E.P.J., 1976, in Structure and Evolution of Close Binary Systems (IAU Symp. 73), eds. P. Eggleton, S. Milton, & J. Whelan (Dordrecht: Reidel), 35.
- van der Hucht, K.A., 2001, New Ast. Rev., 45, 135 (vdH01)
- van der Hucht, K.A., Cassinelli, J.P., & Williams, P.M., 1986, A&A, 168, 111 (vdH86)
- Waldron, W. & Cassinelli, J.P., 2001, ApJ, 548, L45
- Wessolowski, U., 1996, MPE Report 263 (MPE: Garching), 75
- White, R.L., 1985, ApJ, 289, 698
- Willis, A.J. 1996, Ap&SS, 237, 145
- Willis, A.J. & Stevens, I.R., 1996, A&A, 310, 577
- Wright, A.E. & Barlow, M.J., 1975, MNRAS, 170, 41

Fig. 1.— Smoothed EPIC-PN image of the region within  $\approx 3'$  of WR 110 (arrow). *Left*: Broad-band (0.3 - 10 keV). *Right*: Hard-band (6 - 10 keV).

Fig. 2.— Broad-band (0.3 - 10 keV) background-subtracted EPIC-MOS light curve of WR 110 obtained by summing data from the MOS-1 and MOS-2 detectors. Error bars are  $1\sigma$  and the binsize is 512 s. Solid line is the best-fit model for an assumed constant count-rate source.

Fig. 3.— Background-subtracted EPIC-PN spectrum of WR 110 rebinned for display.

Fig. 4.— Differential emission measure (DEM) model of WR 110 based on a fit of the background-subtracted EPIC-PN spectrum using the Chebyshev polynomial algorithm C6PVMKL. Solid line uses canonical WN abundances (vdH86) and dashed line shows the same model using solar abundances (Anders & Grevesse 1989).

Fig. 5.— Unfolded rebinned EPIC-PN spectrum of WR 110 (solid line), overlaid with a cool optically thin VMEKAL plasma model with  $kT = 0.55$  keV and  $N_H = 1.1 \times 10^{22}$  cm $^{-2}$  (dashed line). Abundances of Fe, Si, and S have been varied to fit the emission line profiles. Note the significant hard excess above  $\sim 3$  keV.

Fig. 6.— Cleaned 22 GHz VLA image of WR 110 obtained on 26 Dec 1999. The image is based on  $\approx 30$  min of on-source time acquired in three scans of 10 min each. The deconvolved beam size (lower right) is FWHM =  $0.^{\circ}6 \times 0.^{\circ}3$ . The *rms* noise ( $1\sigma$ ) is 0.15 mJy and contour levels are  $(-3, 3, 6, 9, 12, 15, 18, 21)\sigma$ .

Fig. 7.— The radio spectral energy distribution of WR 110 based on total fluxes measured in near-simultaneous observations at 4.86, 8.44, 14.94, and 22.46 GHz on 26 Dec 1999. The solid line is a best-fit power-law model, which gives a spectral index  $\alpha = +0.64 \pm 0.10$  (90% confidence).

Fig. 1.—

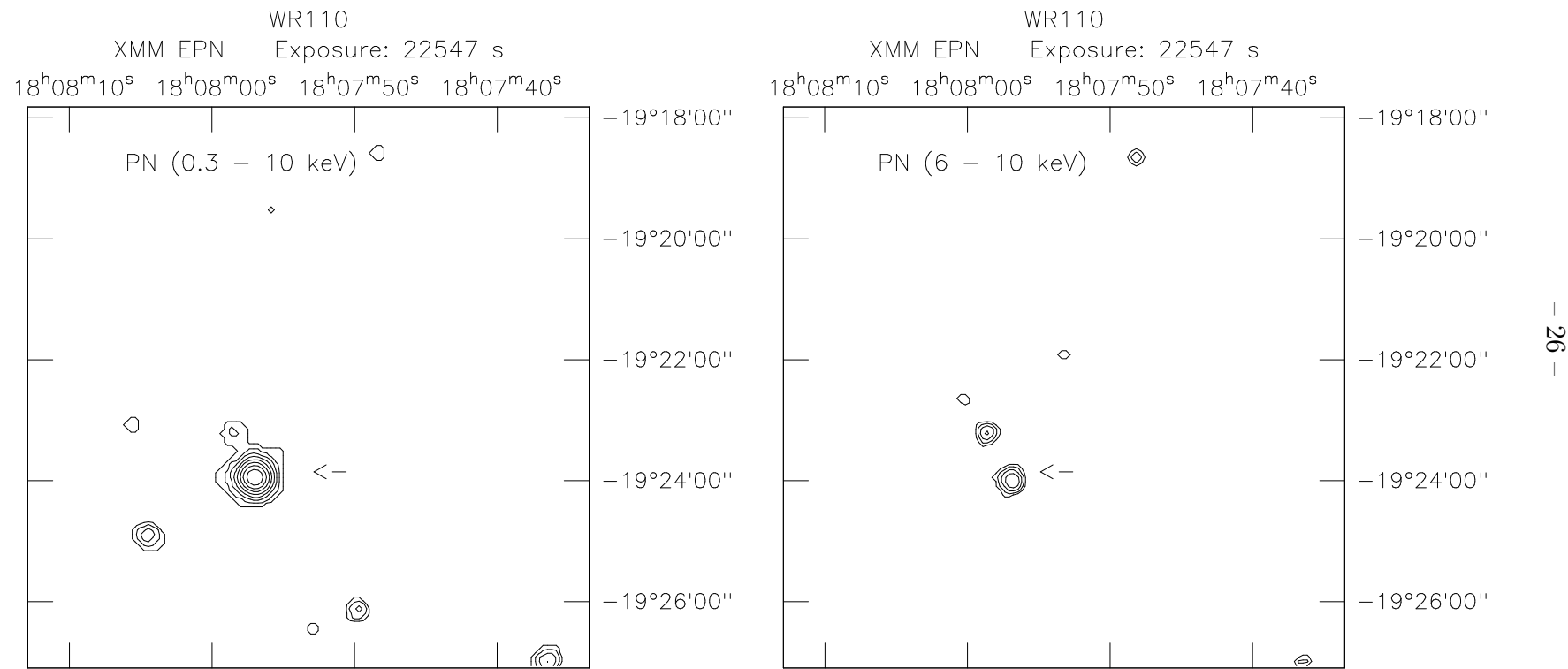
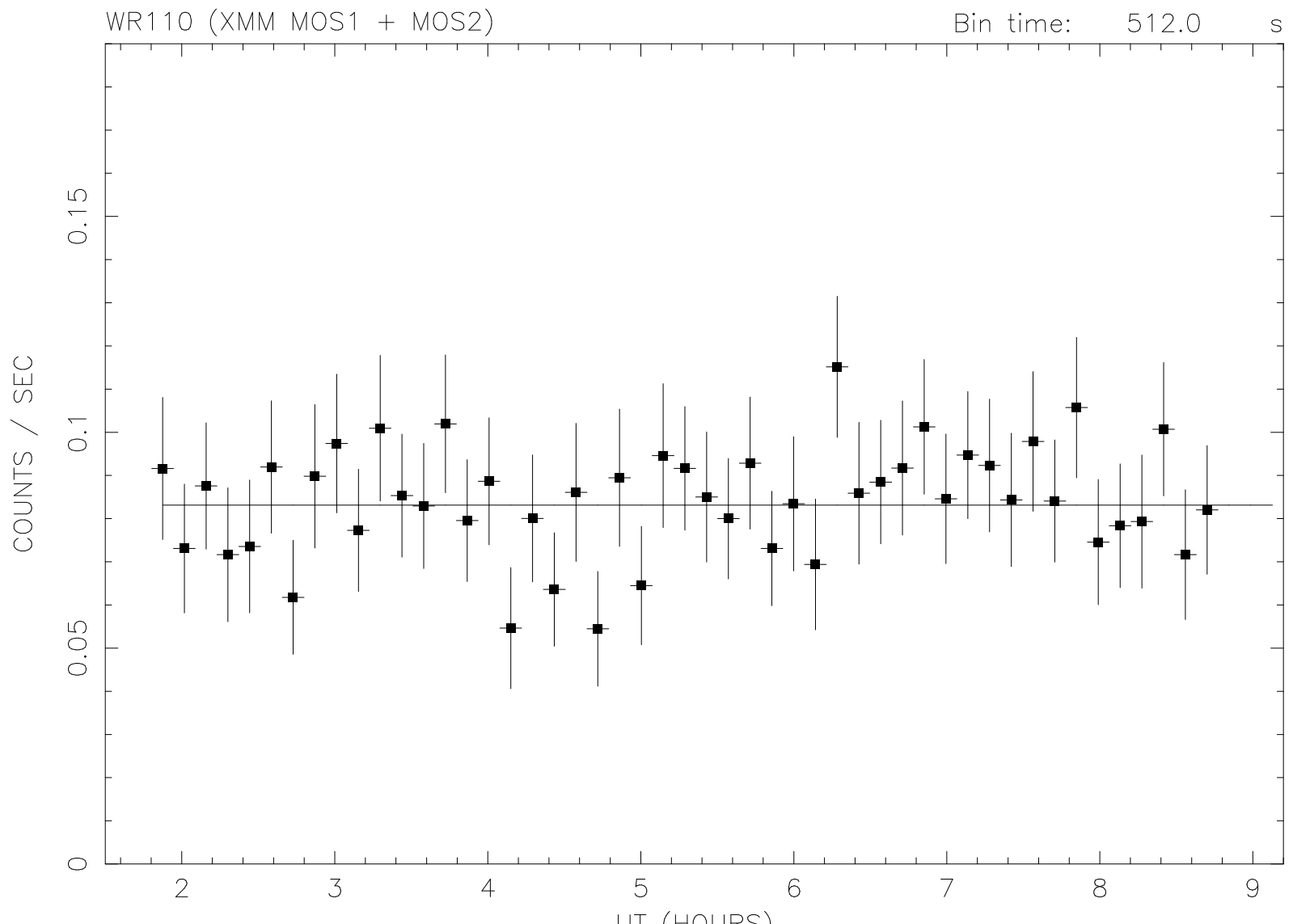
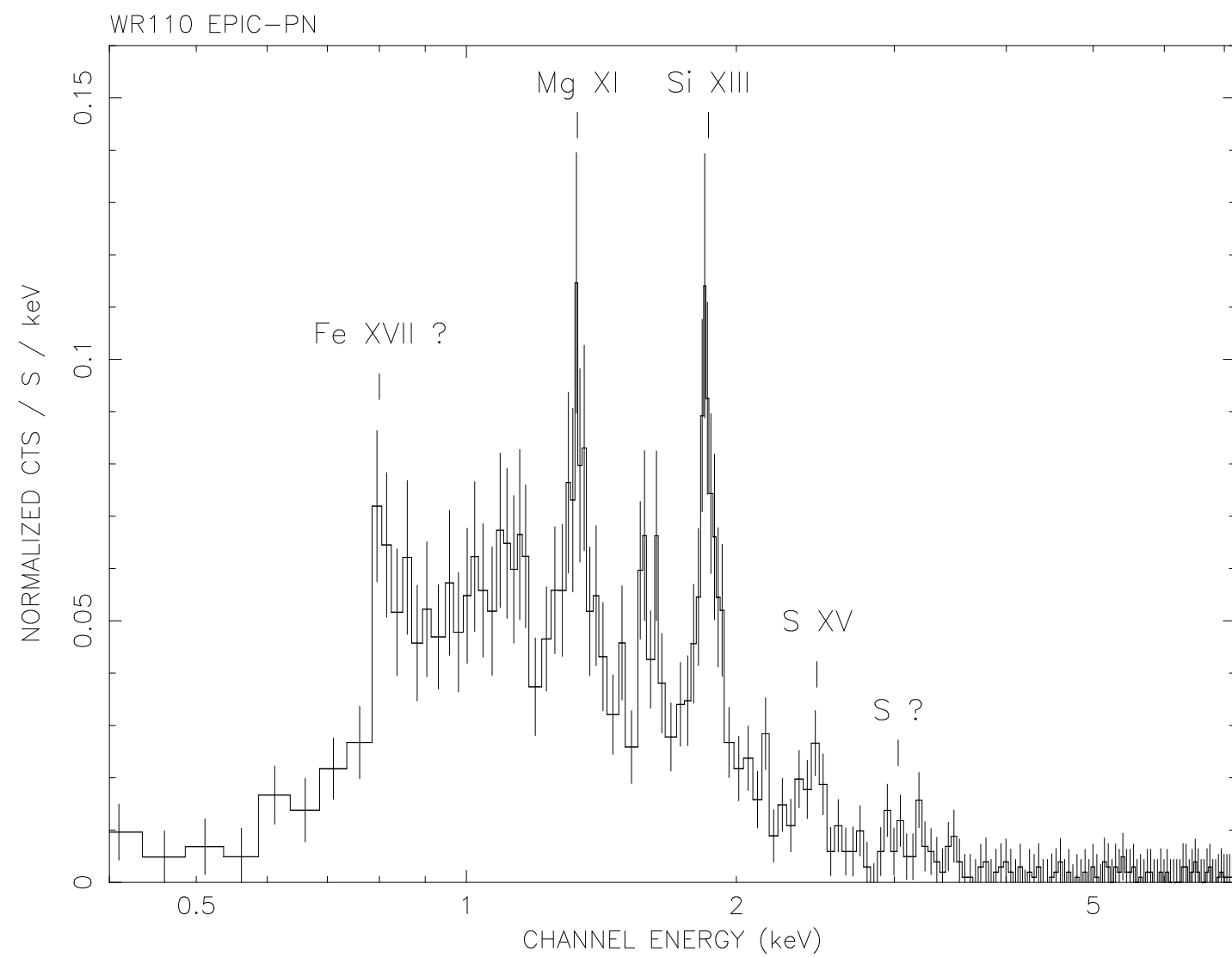


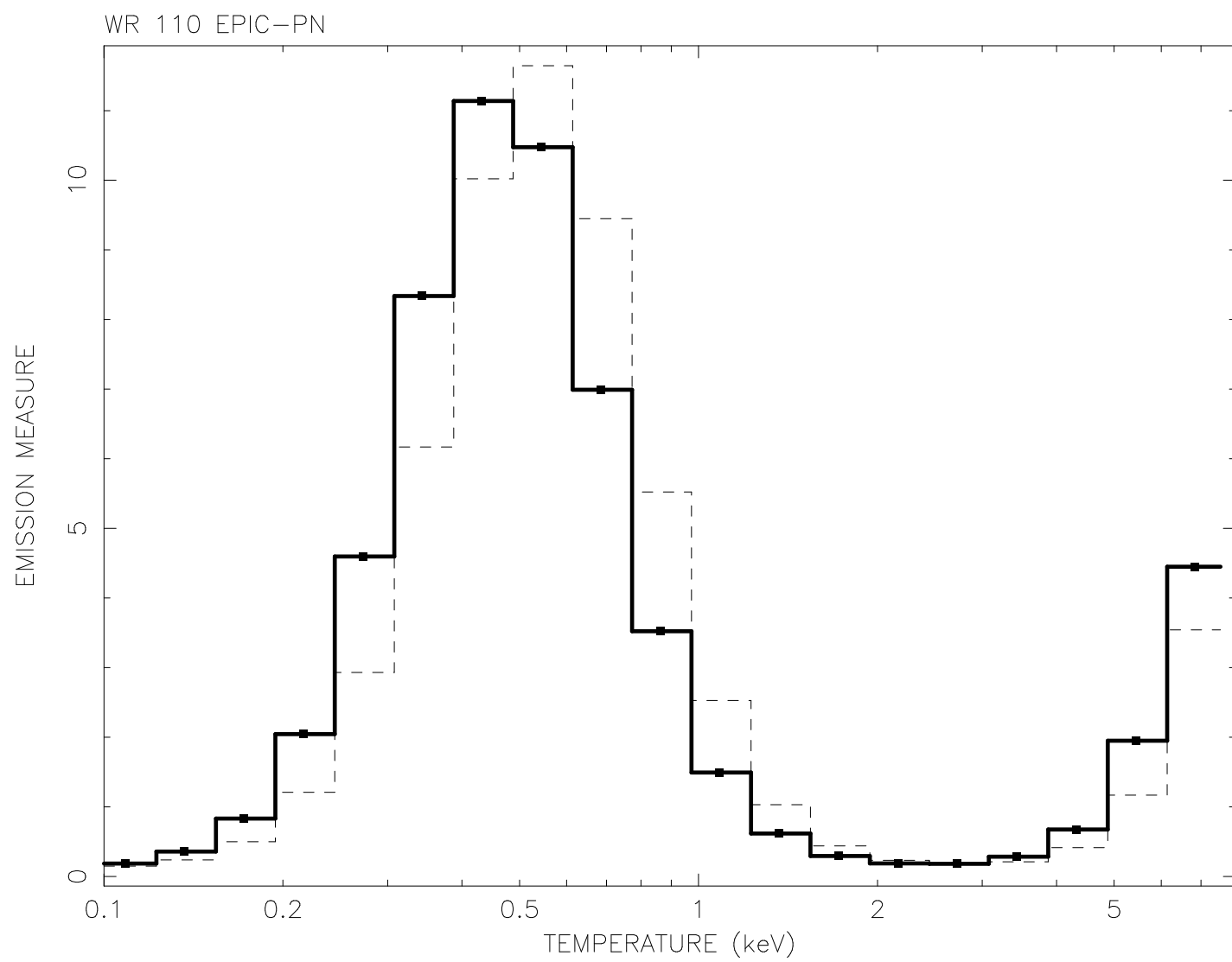
Fig. 2.—



Start Time 11990 1:52:28:608 Stop Time 11990 8:42: 4:608

skimmers 31-Aug-2001 15:00 [1]





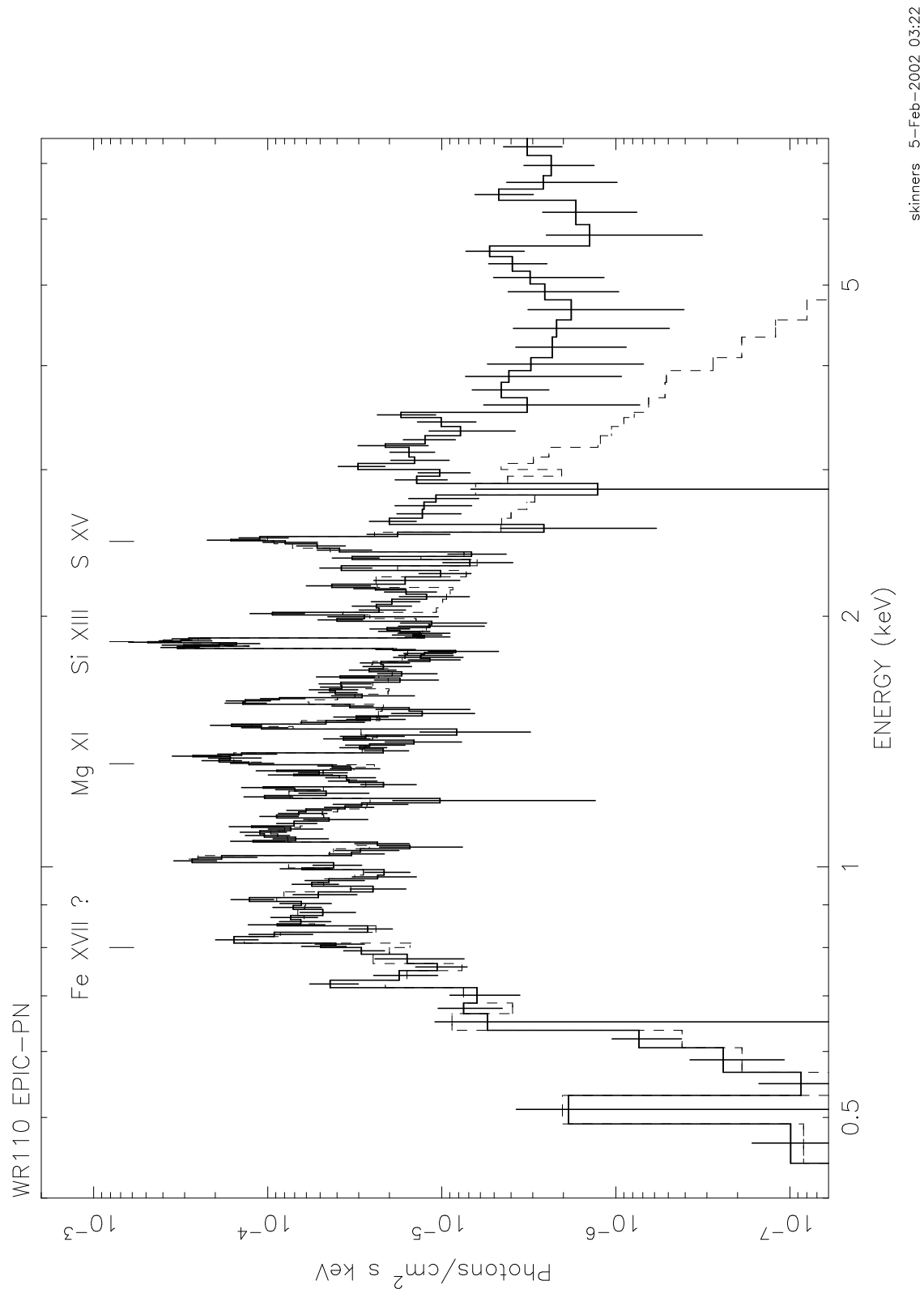


Fig. 5.—

Fig. 6.—

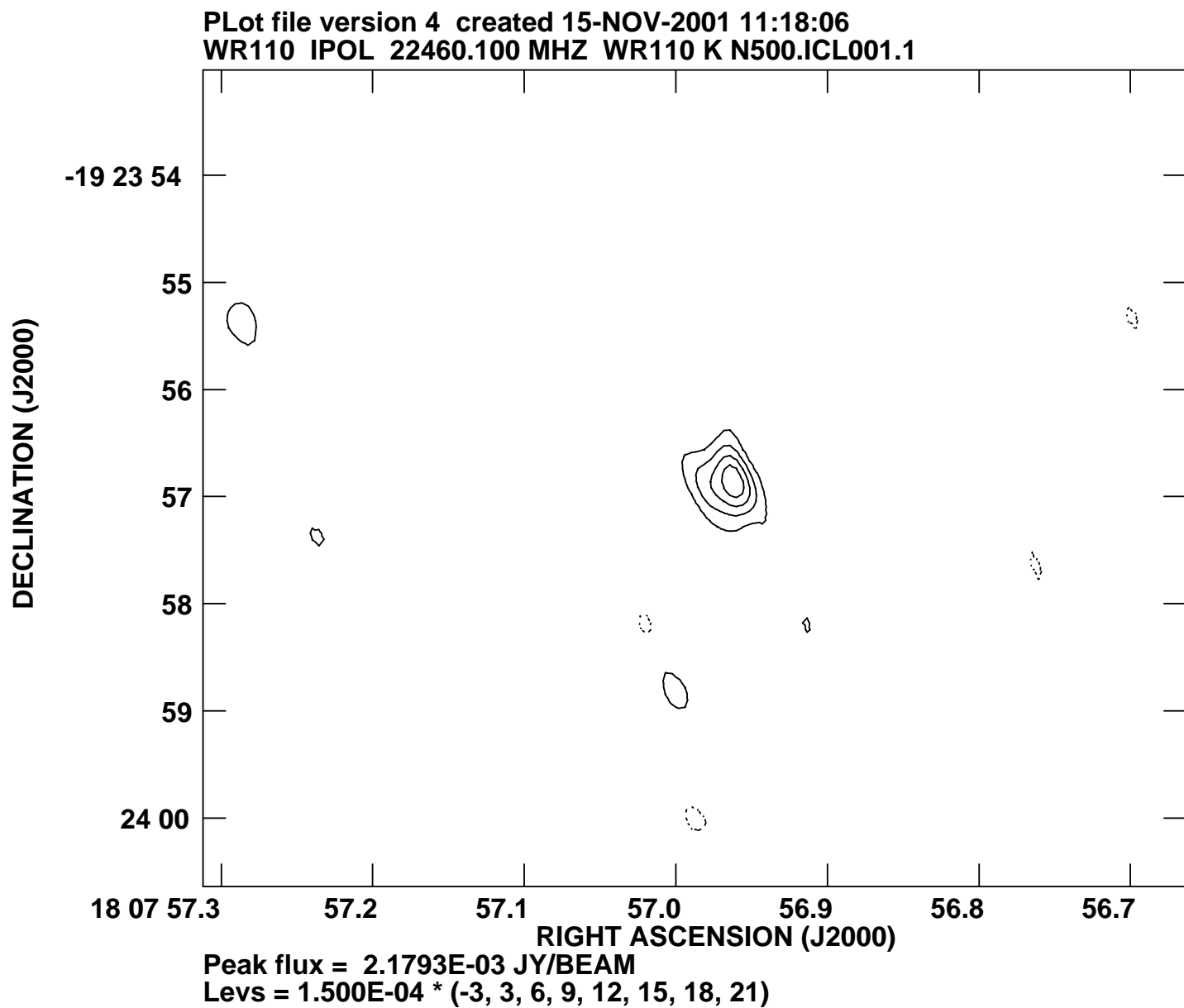
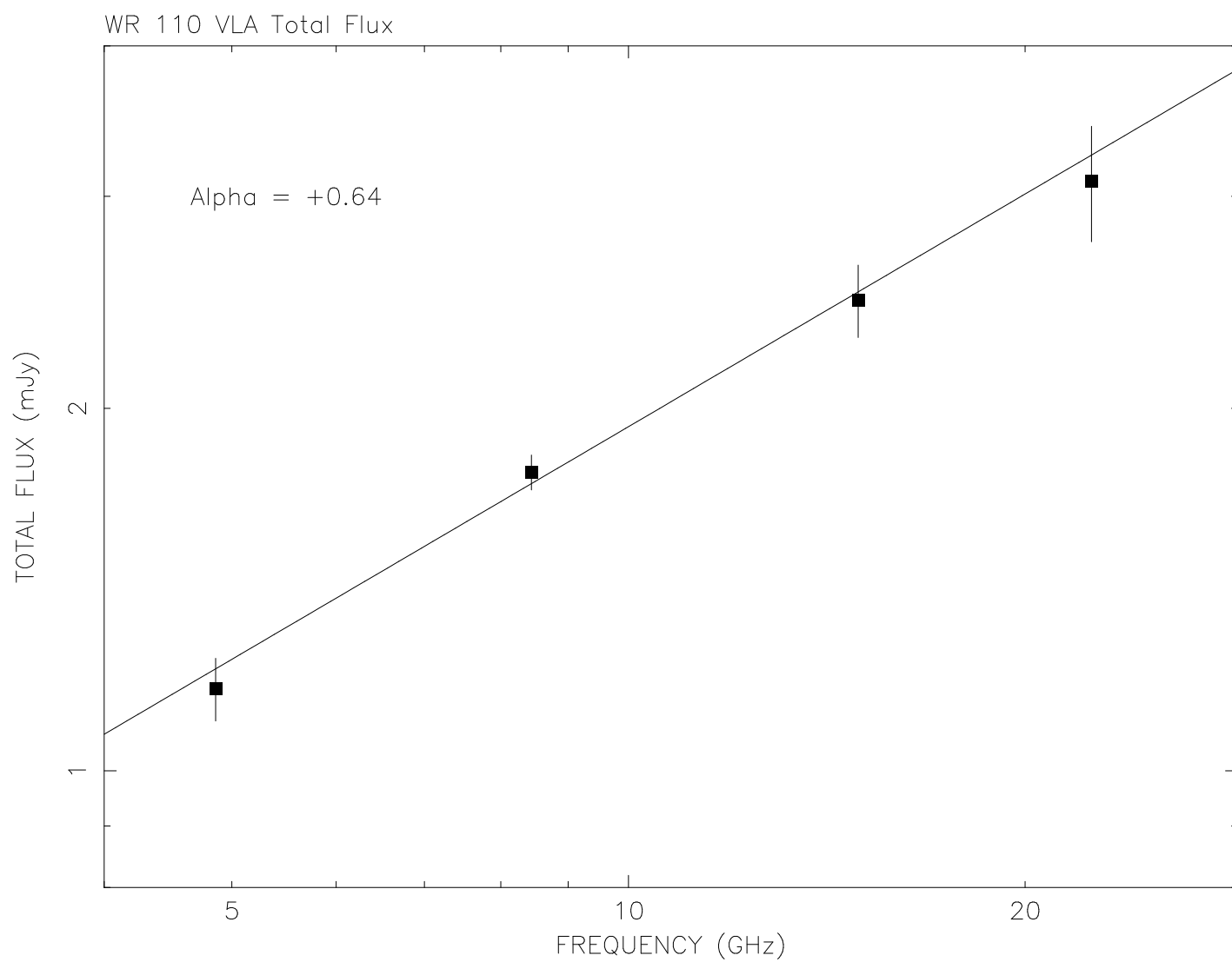


Fig. 7.—



skinners14 [Aug 2001 11:47:11]